Journal of Biomedical Optics

SPIEDigitalLibrary.org/jbo

High temperature heat source generation with quasi-continuous wave semiconductor lasers at power levels of 6 W for medical use

Takahiro Fujimoto
Yusuke Imai
Kazuyoku Tei
Shinobu Ito
Hideko Kanazawa
Shigeru Yamaguchi

SPIE

High temperature heat source generation with quasi-continuous wave semiconductor lasers at power levels of 6 W for medical use

Takahiro Fujimoto,[a,b,d] Yusuke Imai,[b] Kazuyoku Tei,[b] Shinobu Ito,[c,d] Hideko Kanazawa,[d] and Shigeru Yamaguchi[b]
[a]Clinic F, 6-6-1-4F Koujimachi, Chiyoda-ku, Tokyo 102-0083, Japan
[b]Tokai University, Faculty of Science and Technology, Kitakaname 4-1-1, Hiratsuka, Kanagawa 259-1292, Japan
[c]I.T.O. Co. Ltd., 1-6-7-3F Naka-cho, Musashino-shi, Tokyo 180-0006, Japan
[d]Keio University, Division of Physical Pharmaceutical Chemistry Faculty of Pharmacy, 1-5-30 Shibakoen, Minato-ku, Tokyo 105-8512, Japan

Abstract. We investigate a technology to create a high temperature heat source on the tip surface of the glass fiber proposed for medical surgery applications. Using 4 to 6 W power level semiconductor lasers at a wavelength of 980 nm, a laser coupled fiber tip was preprocessed to contain a certain amount of titanium oxide powder with a depth of 100 μm from the tip surface so that the irradiated low laser energy could be perfectly absorbed to be transferred to thermal energy. Thus, the laser treatment can be performed without suffering from any optical characteristic of the material. A semiconductor laser was operated quasi-continuous wave mode pulse time duration of 180 ms and >95% of the laser energy was converted to thermal energy in the fiber tip. Based on two-color thermometry, by using a gated optical multichannel analyzer with a 0.25 m spectrometer in visible wavelength region, the temperature of the fiber tip was analyzed. The temperature of the heat source was measured to be in excess 3100 K. [DOI: 10.1117/1.JBO.19.10.101502]

Keywords: glass fiber; high temperature generation; semiconductor laser.

Paper 130165SSPR received Mar. 22, 2013; revised manuscript received Jul. 19, 2013; accepted for publication Jul. 23, 2013; published online May 22, 2014.

1 Introduction

Coherent light was used to repair detached retinas immediately after the invention of the ruby laser by Maiman in 1960. Thus, the history of medical lasers is over half a century long and it closely follows the development of lasers. Medical laser applications can be broadly divided into two areas: diagnostics in which laser-based sensors provide a great variety of useful information for cancer diagnosis and analyzing cells, and surgery where coherent light is exploited as an energy source that can be concentrated on a tiny location; it is now widely used in surgery and other treatment modalities. Since basic research was initiated with the specific objective of laser surgery applications, almost every coherent source employed in engineering fields has been used in medicine.

Ablating or cutting through living tissue requires a certain power. Nd:YAG, Er:YAG, and CO_2 lasers have been used for these purposes. Recently, semiconductor lasers have also reached intensities that enable them to cut living tissue. Semiconductor lasers will make it quite convenient to channel light through optical fibers that are about 0.1 mm in diameter. In recent years, it has become increasingly common to use fiber-delivered laser light to assist lipolysis,[1–3] percutaneous laser disk decompression,[4–6] and other ablation therapy treatments. Semiconductor lasers do not require dangerously high voltages and their total volumes are relatively compact, making them quite convenient for physicians to carry. Consequently, the number of physicians who use lasers for treatment is expected to continue to rise.

This study describes basic research into generating high temperatures at the tip of a fiber using a semiconductor laser that has a power of several watts. Until now, laser surgery has generally used high-power sources whose emissions are absorbed by tissue, generating high temperatures and a cutting action. Such laser systems are bulky due to the size of the source. This study proposes using 4 to 6 W semiconductor lasers whose emission wavelength is not absorbed by tissue. Instead, the laser output is absorbed by the tip of an optical fiber, thereby generating a relatively small high-temperature region. This study employs a 980-nm diode laser that is less expensive than other lasers used in medical applications and has a simple construction. This report presents an analysis of the emission spectrum at the modified tip of the optical fiber. The first use of this technology has been to drill holes in human bone, but we expect it to be valuable for a wide variety of laser surgeries in the future.

2 Experimental Apparatus

2.1 *Laser and Titanium Powder Used*

Table 1 provides the oscillation conditions of the medical laser system (Jeisys D-30, Gwangmyeong, Korea). Figure 1 shows scanning electoron microscope (SEM) images of the titanium oxide (TiO_2) powder used to create the fiber tip at various magnifications.

Address all correspondence to: Takahiro Fujimoto, Clinic F, 6-6-1-4F Koujimachi, Chiyoda-ku, Tokyo 102-0083, Japan. Tel: +81-3-3221-6461; Fax: +81-3-3221-6462; E-mail: fujimoto@clinic-f.com

Table 1 Specifications of semiconductor laser source and optical fiber.

Laser	Semiconductor	
Wavelength/Mode	980 nm	Multimode
Power	1–30 W	
Operation Mode	Continuous	
	Repetitively pulsed	On time 1–1000 ms
		Off time 1–1000 ms
Fiber	SiO_2	
Mode/Core diameter	Multimode	400 μm
Numerical Aperture	0.39	

2.2 *Fiber Tip Modification by* TiO_2 *Powder*

First, a multimode optical fiber was cut using an optical fiber cutter. The fiber tip was pressed into a sheet of TiO_2 powder (diameter: 10 to 50 μm; molecular weight: 79.88; Rutile type crystals, Wako Pure Chemical Industries, Osaka, Japan) as coherent light was directed through the fiber at several watts for about 200 ms. The tip is heated by scattering absorption of the beam by the TiO_2 powder, which burns the fiber cladding off the tip. The core is heated and fuses and then TiO_2 adheres to the core as it resolidifies.

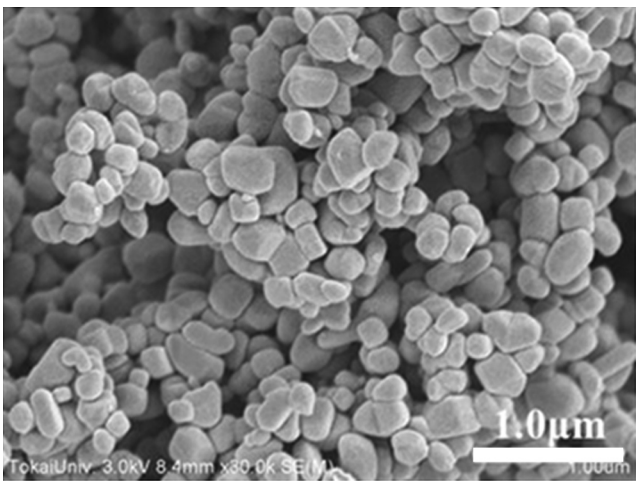

Fig. 1 SEM image of TiO_2 powder.

Figure 2 shows a SEM micrograph of the fiber tip. Quartz fibers are known to melt at a temperature of 1996 K and above. Figure 2(a) shows that the cladding has melted. Since a portion of the fiber was also damaged, the temperature must have exceeded the fusing temperature.

Repeating this experiment with different laser parameters revealed that good TiO_2 deposition was obtained on a multimode optical fiber with a 400-μm diameter core when a pulse with a power of 6 W (intensity: ~2 kW/cm^2) and a duration of 50 ms was used. Illuminating this fiber, which we term as the tip-processed (TP) fiber, with a laser beam generates a relatively small region that has a sufficiently high temperature that it glows; this was highly repeatable. Figure 2(b) shows a photograph of a fiber tip after illumination at ~6 W for 180 ms after withdrawing it from the TiO_2 sheet. Fusion is stronger after TiO_2 had been applied to the fiber tip.

Figure 3 shows the distribution of Ti atoms using electoron probe micro analyser (EPMA), performed to reveal the approximate depth of Ti deposition. This analysis was conducted at a high temperature after three illumination cycles with the 6 W laser following Ti deposition. Ti was found to be distributed to depths of about 100 μm from the surface.

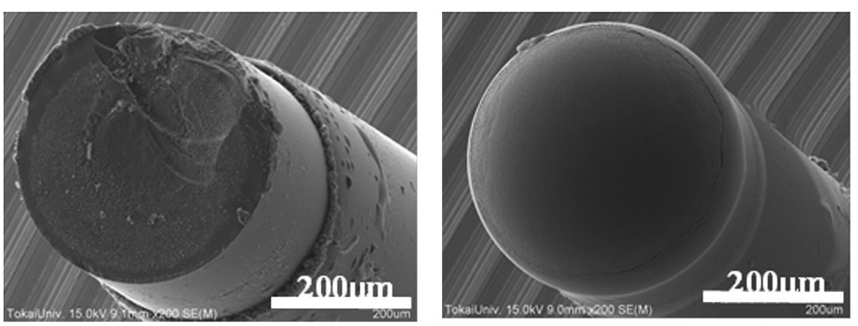

(a) TP Fiber (b) After one fire

Fig. 2 SEM micrograph of the fiber tip. (a) Photograph of the fiber cladding has melted. Since a portion of the fiber was also damaged, the temperature must have exceeded the fusing temperature. (b) Photograph of a fiber tip after illumination at ~6 W for 180 ms after withdrawing it from the TiO_2 sheet. Fusion is stronger after TiO_2 had been applied to the fiber tip.

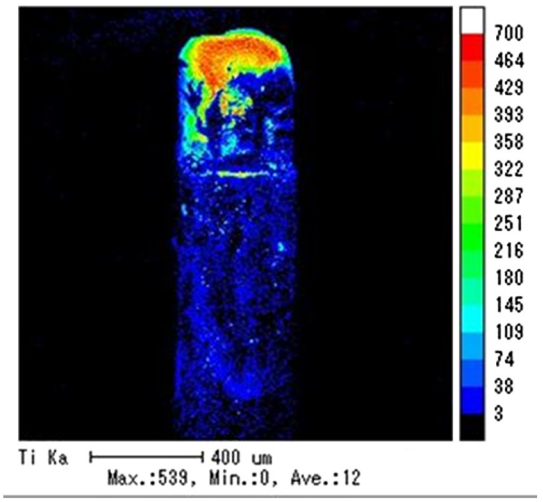

Fig. 3 Longitudinal section of the TP fiber (Ti EPMA). The distribution of Ti atoms using EPMA performed to reveal the approximate depth of Ti deposition. This analysis was conducted at a high temperature after three illumination cycles with the 6 W laser following Ti deposition. Ti was found to be distributed to depths of about 100 μm from the surface.

2.3 *Test Equipment for Observing Temporal Variations in Tip Spectrum*

Figure 4 shows a schematic diagram of the system used to measure the emission brightness and the temperature generated at the TP fiber tip. After depositing TiO_2, the fiber tip was irradiated several times with laser pulses, resulting in the generation

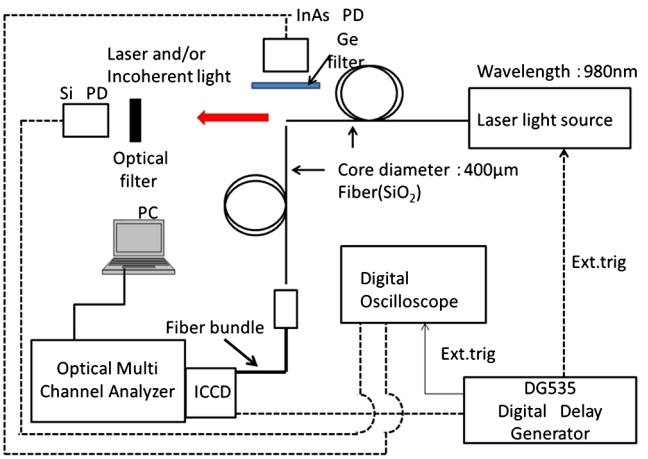

Fig. 4 Experimental schematic of spectroscopic diagnostics of tip-processed (TP) fiber. PD: photovoltaic photodiode, PC: personal computer. Synchronization between laser system and diagnostic system is controlled by a digital delay pulse generator (SRS DG 535). An optical filter is placed in front of a four-stage thermoelectrically cooled InAs PD with a preamplifier, resulting in incoherent radiation being observed from the elevated temperature TP fiber in the infrared wavelength region between 1.9 and 3.2 μm. The high temperature TP fiber radiation in the visible wavelength region between 400 and 800 nm is also observed by a spectrometer with an image intensified CCD time-resolved optical multichannel analyzer. For visible radiation measurements, a 400 μm core optical fiber is used to couple the incoherent radiation into the spectrometer. The infrared signal from the InAs PD (EG&G Judson, J12TE3) is recorded by a digital oscilloscope with 2 Gs and 16-bit resolution (Agilent, 54642A). Both infrared and visible signals are processed by the PC.

of a quite repeatable and stable high-temperature region. The light generated by the superheated fiber tip was examined by both visible and infrared spectra. The visible spectrum was measured using an optical multichannel analyzer (Oriel Instruments, 77702), which could be controlled by a gate. An image intensifier was attached to the analyzer. The light was transferred to the analyzer by an optical fiber bundle. By employing a combination of optical fibers, the measurable range was 400 to 850 nm with a resolution of 1 nm. The system sensitivity was constant throughout the 450 to 650 nm range, so that a band was examined during these measurements.

Simultaneously with these spectral observations, temporal variations in the beam from the 980-nm excitation semiconductor laser were observed using a Si photodetector (New Focus, 1621) equipped with an optical filter; these observations were performed directly in front of the TP fiber. Temporal variations in the infrared from the fiber was observed from the side using an InAs infrared photodetector (Judson, J12TE3) with a Ge optical filter attached to its front. The photodetector with the Ge filter provided a spectrally integrated sum of the intensities of the infrared wavelengths from about 2 μm to the cut-off wavelength of about 3.2 μm. The wave profile was observed on a digital storage oscilloscope (Agilent, 54642A). Trigger was controlled with a delayed pulse oscillator (SRS, DG535) to synchronize the light source, the time-resolving spectrometer, and the oscilloscope.

2.4 *Detection of Electron Spin Resonance Spectra in Mouse Skin after TP Fiber Laser Irradiation*

In the detection by electron spin resonance (ESR) spectra using the DPPMPO (the latest high sensitivity spin trap agent) of mouse skin after TP fiber laser irradiation, we have succeeded in observation of the ESR spectra of the three. Those were the superoxideanion radical (O_2*), hydroxyl radical (OH*) and ascorbyl radical (AsA*). Multiple standard free radicals were generated, and the g-value and hyperfine coupling constant (hfcc) of each spin adduct were 3 obtained by the ESR-spin trapping method to identify the various free radicals. The spin trapping agents used were 5-(diphenylphosphinoyl)5-methyl-4,5-dihydro-3H-pyrrole-*N*-oxide (DPPMPO). The signal ratio was obtained for each sample by comparison with the signal of MnO, an internal standard. The relative intensity of radicals was calculated by comparison with the third MnO signal intensity. The g-value and distance (mT) between the peaks for hfcc were measured by software supplied with the ESR equipment, ESR spectrometer (JEOL, JES-FA200 spectrometer, Tokyo), ESR universal cavity (JEOL, ES-UCX2: TE11 mode cavity) with X-band microwave units (8.750 to 9.650 GHz), an ESR standard marker with manganese oxide (MnO) powder (JEOL DATUM, MO7-FB-4), an aqueous sample cell (JEOL, ES-LC12), sample volume: 20 to 100 μl, a tissue-type: quartz cell (Labotec, Tokyo) with a self-made cover glass ($40 \times 5 \times 0.5$ mm). The spin trapping agents used for ESR were DPPMPO (50 to 500 mM, 10%, w/w dimethyl sulfoxide solution). DPPMPO (100 mg/cm^2) was applied to the irradiation spot before laser irradiation. The irradiated skin tissue was immediately removed and placed on an ice-cold plate after being rinsed with ice-cold phosphate-buffered saline (pH 7.2). The skin tissues including the dermis and epidermis were cut to samples measuring 3 to 5 mm $\times$ 10 to 20 mm. The slice weight was measured before removal to normalize the ESR signal of each radical. The same spin trap agent (10 to 50 μl) was added to the

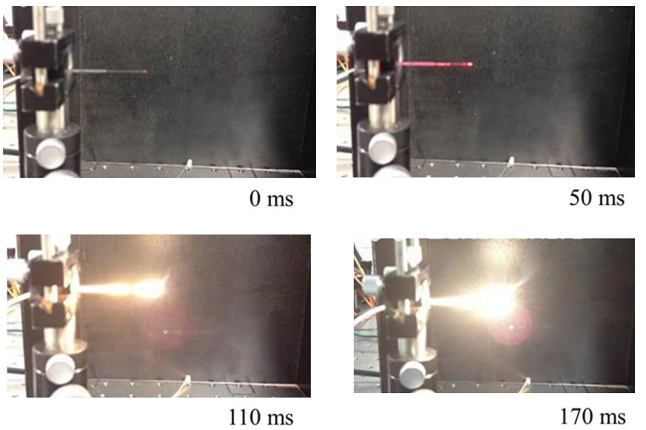

Fig. 5 Image of firing time (ms). The excitation laser and emission from the TP fiber tip for a laser power of 6 W and a pulse width of 180 ms.

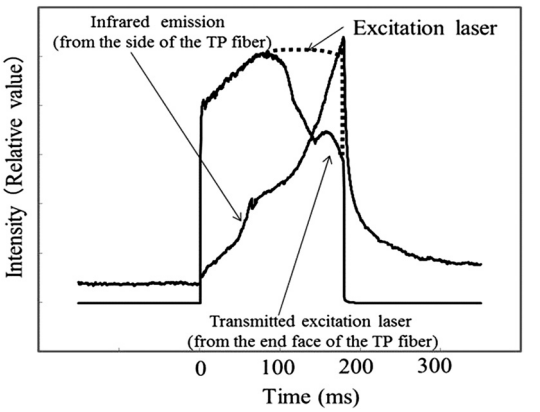

Fig. 6 The variations with time of the excitation laser transmission and the TP fiber tip emissions.

tissue samples (10 to 50 mg) immediately after being weighed, and after precisely 5 min, samples were measured using ESR. To identify the peaks, the signals were analyzed by specialized analysis software installed in the ESR device (ESR computer software, A-System vl.40 ISAJ, FA-manager vl.20, JES, Tokyo, Japan) to determine the g-value and hfcc from the distance between peaks. The data were analyzed using the least significant difference test. One-way analysis of variance was used to determine variance among the data. All data are reported as means $\pm$ srandard error (SE). Statistical significance was set at $P < 0.05$.

3 Results and Discussions

3.1 *Temporal Variations in Emissions from TP Fiber*

Figure 5 shows the passage of a pulse from the excitation laser and emission from the TP fiber tip for a laser power of 6 W and a pulse length of 180 ms.

When the excitation laser was operated at powers too low for visible emission to be measured (<1 W), the power of the beam passing through the filters was just 3% of the excitation power. Depositing TiO_2 to a depth of 100 μm on the fiber tip was estimated to give an absorption coefficient of about 1.75×10^4 m^{-1}. Considering that quartz optical fibers typically have an absorption coefficient of 0.4 m^{-1}, the addition of TiO_2 to the tip increased this parameter by a factor of over 10^5.

Figure 6 shows the variations with time of the excitation laser transmission and the TP fiber tip emissions. The wave in this figure is the time waveform of intensity of some components of the lateral infrared spectrum observed with the InAs photodetector. The intensity of the excitation laser transmission measured by the Si photodetector in front of the fiber tip increased slowly during the first 90 ms of excitation, reflecting the waveform of the output-time characteristics. For a tip that had not been coated with TiO_2, the excitation laser showed a constant intensity after that initial period (dotted line).

However, the transmission from the laser via the TP fiber during the latter 90 ms showed an abrupt reduction due to either abrupt dispersion or absorption of the excitation laser. Since almost no variation was found in the dispersion of the excitation laser measured from the side, we infer that the laser beam was absorbed by the TP fiber tip.

While the excitation laser transmission decreased, the intensity of the infrared emission from the TP fiber increased after about 130 ms. From these temporal changes in the light intensity, we infer that there are two stages in the heating of the TP fiber tip by the excitation laser due to variations in the absorptivity. The first stage is during the initial 110 ms, whereas the second phase is during the subsequent 70 ms (approximate values).

Figure 7 shows the spectra measured 50, 80, 110, 140, and 170 ms after the onset of illumination by the excitation laser. Sufficient infrared light was emitted for a signal immediately after illumination by the excitation laser, but the intensity of the visible beam was barely observable 50 ms after emission started. The beam intensity did not increase sharply until 110 ms. If this is assumed to be black-body radiation, this suggests that the visible beam components suddenly increase, implying that the TP fiber tip exceeds about 3000 K at about 110 ms. The TP fiber temperature increases gradually as the deposited TiO_2 originally absorbed into the fiber core under the excitation laser during the initial stage is now absorbed by Si in the core fiber, which has been thermally ionized. When the temperature exceeds 2800 K and SiO is generated by the SiO_2 making up the fiber, the light absorption rate increases many times. Nearly all the optical energy is converted to thermal energy in the ultrathin (200-μm thick) region at the tip of the TP fiber, sharply increasing the temperature of the TP fiber.

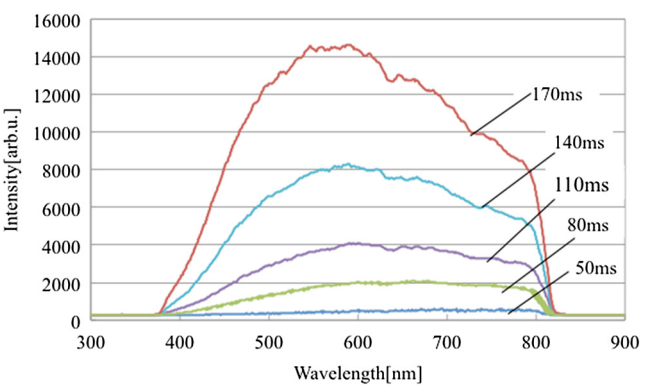

Fig. 7 The spectra measured 50, 80, 110, 140, and 170 ms after the onset of illumination by the excitation laser. Sufficient infrared light was emitted for a signal immediately after illumination by the excitation laser, but the intensity of the visible beam was barely observable 50 ms after emission started.

The temperature of the hottest portion of the TP fiber was estimated using the ratio temperature method. Planck's radiation law provides the following expression for the radiative energy density per unit volume and wavelength,

$$dW = \frac{8\pi hc}{\lambda^5}\frac{1}{\exp(hc/k\lambda T)-1}d\lambda, \tag{1}$$

where h is Planck's constant, c is the velocity of light, λ is the wavelength of the electromagnetic wave, k is Boltzmann's constant, and T is the temperature.

The ratio temperature method is an effective way for measuring the temperature when the emissivity of the observed object is unknown and when we wish to avoid considering the transmissivity of the glass or other material lying between the observed object and the measuring instrument. Using the time series for the emission intensities at wavelengths 1 and 2 obtained by the frequency- and time-resolved measurements by the optical multi-channel analyzer, the following expression is found for the fiber tip temperature. We apply Planck's radiation law for a real high-temperature region to find

$$M_\lambda = \frac{\tau\varepsilon c_1}{\lambda^5 e^{\frac{c_2}{\lambda_1 T}}} = \tau\varepsilon c_1 \lambda^{-5} e^{\frac{c_2}{\lambda_2 T}}, \tag{2}$$

where c_1 is the first radiation constant ($= 3.741844\times 10^{-16}$ W $\cdot$ m^2), λ is the wavelength in μm, c_2 is the second radiation constant ($= 1.438769\times 10^{-2}$ m $\cdot$ K), T is the absolute temperature (K), τ is the transmissivity, and ε is the emissivity. If the radiation intensities (quantities of radiation) at wavelengths λ_1 and λ_2 are, respectively, denoted M_1 and M_2, then the ratio R of M_1 to M_2 is defined as

$$R = \left(\frac{M_1}{M_2}\right) = \frac{\tau_1}{\tau_2}\frac{\varepsilon_1}{\varepsilon_2}\frac{\lambda_2^5}{\lambda_1^5}\frac{e^{\frac{c_2}{\lambda_2 T}}}{e^{\frac{c_2}{\lambda_1 T}}}. \tag{3}$$

Taking the logarithm of both sides, we obtain

$$\ln R = \ln\left(\frac{\tau_1}{\tau_2}\right) + \ln\left(\frac{\varepsilon_1}{\varepsilon_2}\right) + 5\ln\left(\frac{\lambda_2}{\lambda_1}\right) + \frac{c_2}{T}\left(\frac{1}{\lambda_2}-\frac{1}{\lambda_1}\right). \tag{4}$$

Here, the emissivities ε_1 and ε_2 are nearly identical, so $\varepsilon_1/\varepsilon_2 \approx 1$. If $\tau_1/\tau_2 = 1$ for transmissivities τ_1 and τ_2, then

$$\ln R = 5\ln\left(\frac{\lambda_2}{\lambda_1}\right) + \frac{c_2}{T}\left(\frac{1}{\lambda_2}-\frac{1}{\lambda_1}\right). \tag{5}$$

The temperature T_a is then given by

$$T_a = \frac{c_2\left(\frac{1}{\lambda_2}-\frac{1}{\lambda_1}\right)}{\ln\left(\frac{M_1}{M_2}\right) - 5\ln\left(\frac{\lambda_2}{\lambda_1}\right)}. \tag{6}$$

The temperature was determined from the visible components of 500 and 600 nm, using the ratio of the intensity of these wavelengths and the temporal variations in the visible frequency intensities shown in Fig. 7. The ratio temperature method was applied with the intensity observed between 80 and 170 ms, when visible frequencies were quite bright; this yielded estimates of about 3050 K at about 80 ms and ultimately about 3500 K at 170 ms for the temperature of the fiber tip. Figure 8 shows the temporal variation for the TP fiber tip. Typical temperatures for 80, 110, 140, and 170 ms, after excitation laser pulse was triggered, were measured to be 2540, 2710, 2940 and 3110 K, respectively. After 15 and 30 shots, the temperature of the tip was decreased, respectively.

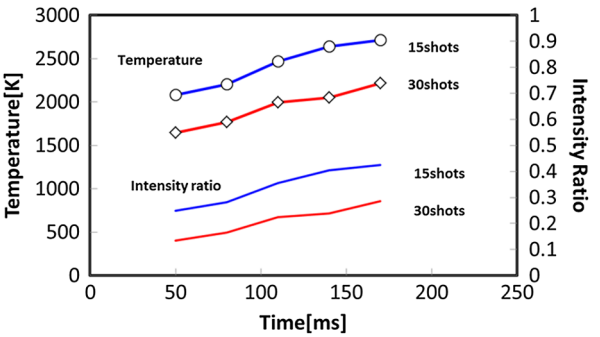

Fig. 8 The temporal variation for the TP fiber tip. Typical temperatures for 80, 110, 140, and 170 ms, after excitation laser pulse was triggered. After 15 and 30 shots, the temperature of the tip was decreased, respectively.

If a portion of a single-mode fiber carrying several watts of optical power is locally heated due to bending or some other factor, a plasma will generally be generated in the core region. This plasma is confined within the optical fiber and damages the core region. The damaged portion then spreads upstream toward the source. This is referred to as fiber fusing. Since optical fibers transmit light beams over long distances, they must be constructed of a highly transparent material. Quartz glass is typically used for optical fibers; it does not deform at temperatures <1870 K. However, a well-known measurement of the temperature dependence of the transmissivity of a 1-m long optical fiber revealed that the absorptivity of quartz increased abruptly in the neighborhood of 1320 K. If a portion of a single-mode optical fiber (core diameter: 10 μm) carrying several watts is heated to about 1270 K, then the portion will become a light absorber and the optical energy will be converted into thermal energy. If we continue to introduce optical energy into the fiber, adjacent portions will also turn into light absorbers. This progression readily advances toward the light source. At the same time, the temperature rapidly increases (to several thousand Kelvin) and eventually, a luminous plasma proceeds through the waveguide structure, approaching a steady state.

Fiber fusing was discovered in the late 1980s,[7] but it was much more commonly observed as the powers of semiconductor lasers increased. If a current with a power of several watts passes through an optical fiber, the fiber will be heated above its fusion temperature (1973 K) due to arcing and other phenomena in a short period of time and fiber fusing will occur around the heated region. The core temperature then rapidly climbs from the original temperature (about 2300 K) by nearly a factor of 10 (over 10,000 K). Kashyap and Blow[7] examined the relationship between the optical absorption coefficient of a Ge-doped quartz optical fiber and the temperature under Nd:YAG illumination (wavelength: 1.064 μm) and found that the optical absorption coefficient increased sharply from 1323 K. According to their measurements, the absorptivity coefficient at 1373 K is about 0.46 m^{-1}. One study on fusing in optical fibers estimated the fiber tip temperature,[8] and other studies have compared fusing models.[9–13] Research has also been

conducted on a contact laser scalpel composed of a conic sapphire tip attached to the tip of a fiber. Coherent light is concentrated at the apex of the tip. Depositing a carbon film at the tip clearly causes a soldering iron effect. Heating procedures that do not require using TiO_2 are expected to be developed in the future.[14] The authors have already used this laser for induction of different reactive oxygen species in the skin during various laser therapies.[15]

The present study has verified that controlling the mode of emission of energy at the tip of an optical fiber causes the beam to be absorbed by a tiny region at the tip and converted into thermal energy. It now appears to be feasible to cause conditions that promote fiber fusing, which will permit surgical tools based on this method to be used clinically.

3.2 *Free Radical Generation by TP Fiber and No TP Fiber Laser Irradiation*

Figure 9 shows the relationship between free radical generation by TP fiber and no TP fiber laser irradiation. ESR spectra were measured according to the method of Ito et al.[16] As a result, TP fiber laser increased the production of O_2*, OH*, and AsA* in the mouse skin significantly compared to the no TP fiber laser irradiation. ** denotes $P < 0.01$, * denotes $p < 0.05$, $n = 8$. This result supported the previous studies[17–20] of increased production of O_2* and OH* by the photocatalytic reaction of titanium oxide in animal cell. In recent years, much research has been done by laser devices in the field of skin rejuvenation. A laser or another visible light device at the energy doses used for skin rejuvenation produces high amounts of reactive oxygen species, which destroy old collagen fibers and kill old skin cells, encouraging the formation of new ones.[21] Additionally, since it was known that these reactive oxygen species like O_2*, OH*, and AsA* can increase skin cell damage,[22] it will be considered to allow efficient removal of skin cell or skin tissue by TP fiber laser irradiation. In other words, this result suggests that TP fiber laser device will be an effective technology to make more compact, low cost and less energy laser device for skin rejuvenation.

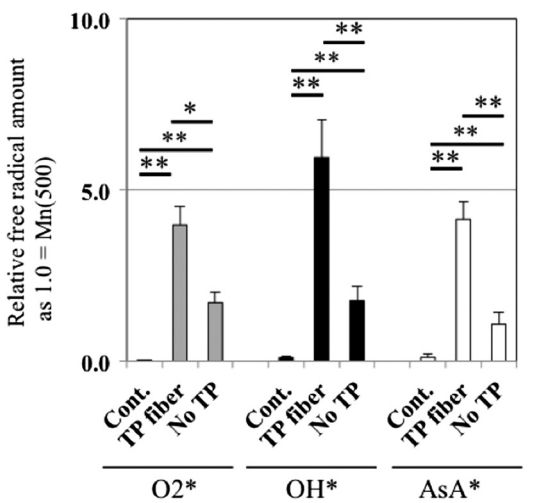

Fig. 9 Free radical generation by TP fiber and no TP fiber laser irradiation. TP fiber laser in creased the production of O2* , OH*, and AsA* in the mouse skin significantly compared to the no TP fiber laser irradiation.

4 Conclusions and Future Perspective

This experiment demonstrates that it is possible to produce a region that is 400 μm in diameter and 200 μm long near the tip of a quartz optical fiber that can generate clinically useful high temperatures of 3500 K. We are currently using a laser system to perform dermatological investigations to measure reactive oxygen species in skin.[14] This study has demonstrated that 4 to 6 W semiconductor lasers can be clinically used in clinics by modifying the fiber tip.

Medical treatments with lasers in recent years have been extended to a variety of fields, including PLDD, which is ablation of disks with a percutaneously inserted fiber laser to relieve nerve compression, and laser-assisted liposuction, in which lasers play a part in sucking fat.

Herniated disk repair operations by conventional surgery require a minimum of 6 weeks for recovery (including hospitalization time) and the patient's quality of life is significantly reduced after the operation. It is quite significant that laser-based PLDD allows the patient to return to a normal life the day after the operation. Since its approval by the USFDA, fiber delivery of a Nd:YAG beam has become an essential component of the toolkit for mesotherapy, permitting treatments such as removal of excessive fat and sagging skin. Titanium oxide powder has a low tendency to cause allergic reactions; it is a common component of emulsions used by clinical physicians for mouthwashes, commercial suntan lotions, food additives, and other products. It is also used for the head of artificial bone. It appears to be quite suitable for use in living tissue.

The chief disadvantage of laser devices used in tissue or for ablative treatments are their size and their cost. The 980-nm semiconductor laser beams are in the near infrared; their low absorption in water makes them difficult to apply for PLDD or laser-assisted liposuction. However, since they do not require dangerously high voltages and the total volume of these devices are relatively compact, they are quite convenient for physicians to carry so that the number of physicians using lasers for treatment is expected to continue to rise.

Acknowledgments

The authors would like to express their deep appreciation to Professor M. Wakaki of Tokai University.

References

1. A. Goldman, D. Schavelzon, and G. Blugerman, "Laser lipolysis: liposuction using Nd:YAG laser," *Rev. Soc. Brasil Cirurgia Plástica* **17**(1), 17–26 (2002).
2. A. Goldman, D. Schavelzon, and G. Blugerman, "Liposuction using neodymium: Yttrium-aluminium-garnet laser," *Plast. Reconstr. Surg.* **111**(7), 2497 (2003).
3. A. Badin et al., "Laser lipolysis: flaccidity under control," *Aesth. Plast. Surg.* **26**(5), 335–359 (2002).
4. P. A. Luijsterburg et al., "Physical therapy plus general practitioners' care versus general practitioners' care alone for sciatica: a randomized clinical trial with a 12-month follow-up," *Eur. Spine J.* **17**(4), 509–517 (2008).
5. G. B. Andersson et al., "Consensus summary of the diagnosis and treatment of lumbar disc herniation," *Spine* **21**(24S), S75–S78 (1996).
6. P. A. Brouwer and B. Schenk, "Percutaneous disc treatment," in *Imaging of the Musculoskeletal System*, T. Pope et al., Eds., Saunders/Elsevier Inc., Philadelphia (2008).
7. R. Kashyap and K. J. Blow, "Observation of catastrophic self-propelled self-focusing in optical fibres," *Electron. Lett.* **24**, 47–49 (1988).
8. Y. Shuto et al., "Fiber fuse phenomenon in step-index single-mode optical fibers," *IEEE J. Quantum Electron.* **40**(8), 1113–1121 (2004).

9. Y. Shuto et al., "Evaluation of high-temperature absorption coefficients of optical fibers," *IEEE Photon. Technol. Lett.* **16**(4), 1008–1010 (2004).
10. D. D. Davis, S. C. Mettler, and D. J. DiGiovani, "A comparative evaluation of fiber fuse models," *Proc. SPIE* **2966**, 592–606 (1997).
11. Y. Shuto, "Evaluation of high-temperature absorption coefficients of ionized gas plasmas in optical fibers," *IEEE Photon. Technol. Lett.* **22**(3), 134–136 (2010).
12. D. P. Hand and P. S. Russell, "Solitary thermal shock waves and optical damage in optical fibers: the fiber fuse," *Opt. Lett.* **13**(9), 767–769 (1988).
13. E. M. Dianov et al., "High-speed photography, spectra, and temperature of optical discharge in silica-based fibers," *IEEE Photon. Technol. Lett.* **18**(6), 752–754 (2006).
14. M. Miyasaka et al., "Basic researches of Nd:YAG laser with contact type scalpel," in *Proc. of the Third International Nd:YAG Laser Symp.*, pp. 634–637, Professional Postgraduate Services, Tokyo (1986).
15. T. Fujimoto et al., "Induction of different reactive oxygen species in the skin during various laser therapies and their inhibition by fullerene," *Lasers Surg. Med.* **44**(8), 685–694 (2012).
16. S. Ito et al., "Differential effects of the ascorbyl and tocopheryl derivative on the methamphetamine-induced toxic behavior and toxicity," *Toxicology* **240**(1–2), 96–110 (2007).
17. B. Shen, J. C. Scaiano, and A. M. English, "Zeolite encapsulation decreases TiO2-photosensitized ROS generation in cultured human skin fibroblasts," *Photochem. Photobiol.* **82**(1), 5–12 (2006).
18. T. Sawada et al., "ESR detection of ROS generated by TiO2 coated with fluoridated apatite," *J. Dent Res.* **89**(8), 848–853 (2010).
19. M. Li, K. J. Czymmek, and C. P. Huang, "Responses of Ceriodaphnia dubia to TiO2 and Al2O3 nanoparticles: a dynamic nano-toxicity assessment of energy budget distribution," *J. Hazard Mater.* **187**(1–3), 502–508 (2011).
20. J. H. Seo et al., "Cytotoxicity of serum protein-adsorbed visible-light photocatalytic Ag/AgBr/TiO2 nanoparticles," *J. Hazard Mater.* **198**, 347–355 (2011).
21. R. Lubart et al., "A reasonable mechanism for visible light-induced skin rejuvenation," *Lasers Med. Sci.* **22**(1), 1–3 (2007).
22. S. Ito et al., "The co-application effects of fullerene and ascorbic acid on UV-B irradiated mouse skin," *Toxicology* **267**(1–3), 27–38 (2010).